accepted by Astrophysical Journal

Gamma–ray Production in Supernova Remnants

T.K. Gaisser
Bartol Research Institute, University of Delaware, Newark, DE 19716

R.J. Protheroe
Department of Physics and Mathematical Physics
The University of Adelaide, Adelaide, Australia 5005

Todor Stanev
Bartol Research Institute, University of Delaware, Newark, DE 19716

ABSTRACT

The bulk of the cosmic rays up to about 100 TeV are thought to be accelerated by the 1st order Fermi mechanism at supernova shocks, producing a power-law spectrum. Both electrons and protons should be accelerated, but their ratio on acceleration is not well known. Recently, the EGRET instrument on the Compton Gamma Ray Observatory has observed supernova remnants IC 443 and γ Cygni at GeV energies. On the assumption that the observed gamma-rays are produced by accelerated particles in the remnants (rather than, for example, from a central compact object) we model the contributions due to pion production, bremsstrahlung, and inverse Compton scattering on the cosmic microwave, diffuse galactic radiation, and locally produced radiation fields. In the case of the same spectral index for both electrons and nuclei, and a cut-off at 80 TeV, we find that a spectral index of accelerated particles close to 2.4, and a ratio of electrons to protons in the range 0.2 to 0.3, gives a good fit to the observed spectra. For lower cut-off energies flatter spectra are possible. We also investigate the case where the electron spectrum is steeper than that of nuclei. We discuss the implications of our results for observations at air shower energies, and for the propagation of cosmic rays.

Subject headings: cosmic-rays — acceleration — gamma ray sources — supernova remnants

1. Introduction

Supernova remnants (SNR) are believed to be responsible for accelerating particles to energies of at least 100 TeV (see e.g. Drury 1983, Blandford & Eichler 1987, Berezhko &

Krymski 1988, Jones & Ellison 1991), and a fraction of the accelerated particles would interact within the supernova remnant and produce gamma–rays (Drury, Aharonian, & Völk 1993). Recent observations above 100 MeV by the EGRET instrument on the Compton Gamma Ray Observatory have found gamma ray signals associated with at least two supernova remnants – IC 443 and γ Cygni (Esposito et al. 1996). Further evidence for acceleration in SNR comes from the recent ASCA observation of non-thermal X–ray emission from SN 1006 (Koyama et al. 1995). Reynolds (1996) and Mastichiadis (1996) interpret the latter as synchrotron emission by electrons accelerated in the remnant up to energies as high as 100 TeV.

In the diffuse galactic background the characteristic π^0 peak at 70 MeV is clearly evident. The power-law spectra, dominated by bremsstrahlung, contribute $\sim 10\%$ at 1 GeV (Hunter et al. 1995, Hunter et al. 1997). The π^0 peak is not so clearly visible, however, in the spectra of IC 443 and γ Cygni, possibly due to the larger error bars. However, this may instead suggest larger bremsstrahlung and inverse Compton (IC) contributions, and a correspondingly higher electron to proton ratio than in galactic cosmic rays. From detailed modeling of the gamma-ray spectra of IC 443 and γ Cygni it should be possible to determine the relative contributions of π^0 decay, bremsstrahlung, and inverse Compton scattering to these spectra, and thereby to obtain information about the conditions in these sources. This would also allow a better determination of the expected extrapolation of the Egret spectra for these sources to the TeV energy range.

Gamma rays are produced by electrons in bremsstrahlung interactions, and by inverse Compton interactions with the cosmic microwave background (Mastichiadis 1996), with the diffuse galactic infrared/optical radiation, and with the radiation fields of the remnant itself. Protons produce gamma rays through the decay of neutral pions produced in proton–nucleus collisions. Drury, Aharonian & Völk (1993) calculated the π^0 decay gamma ray flux expected from supernova remnants due to interactions of accelerated cosmic ray nuclei with matter in the remnant. They calculated the expected flux as a function of supernova age and showed that a number of remnants should be detectable above 100 MeV. Mastichiadis (1996) has included synchrotron radiation and inverse Compton scattering on the cosmic microwave background, and shown that synchrotron radiation by directly accelerated electrons is probably responsible for the non-thermal X–rays observed in SN 1006. Mastichiadis also showed that SNR could produce a flux at TeV energies by inverse Compton scattering which is comparable to that predicted for pion production by Drury, Aharonian & Völk (1993) . An important point of the papers of both Reynolds (1996) and Mastichiadis (1996) is that electrons should be accelerated up to 100 TeV energies. Mastichiadis also suggests that the observation of TeV gamma rays from supernova remnants would not, in itself, provide direct evidence of acceleration of nuclei at supernova shocks. Pohl (1996) has also recently suggested TeV gamma-rays from supernova remnants may be of leptonic origin.

In the present paper we consider gamma-ray production by interactions of accelerated nuclei and electrons in IC 443 and γ Cygni. Our approach is to analyze the observed γ–ray fluxes and attempt to extract the source parameters from the data rather than use theoretical models of particle acceleration in supernova remnants. We assume power law spectra for electrons and

protons, possibly different in slope and in maximum momentum on acceleration. We perform a maximum likelihood fit to the gamma ray spectra of IC 443 and γ Cygni to determine the ratio of electrons to protons, the power-law spectral index, and the average matter density seen by the accelerated particles.

2. Relative importance of pion production, bremsstrahlung and inverse Compton scattering

Before describing our detailed calculation, we first briefly discuss the general features of the expected π^0, bremsstrahlung and inverse Compton gamma ray spectra, and make order of magnitude estimates of their relative contributions to the gamma ray flux. The momentum spectrum of particles accelerated by first order Fermi acceleration at a strong shock is expected to be $dN/dp \sim p^{-2}$. Protons accelerated with this spectrum, and interacting within the remnant, will produce at high energies a π^0 gamma ray number spectrum having approximately the same slope, $\sim E^{-2}$, but with a low-energy turnover at $\sim m_\pi c^2/2$. At high energy, electrons will cool by inverse Compton and synchrotron losses, $dE/dt \propto -E^2$ (neglecting, for the moment, scattering in the Klein-Nishina regime). In an equilibrium situation, the ambient spectrum of electrons will be steepened by one power to $\sim E^{-3}$, giving rise to a spectrum of inverse Compton gamma rays proportional to $\sim E^{-2}$. However, as we shall show below, *a priori* it is not obvious that that such an equilibrium exists for the supernova remnants in question.

The cooling time for electrons in a magnetic field is

$$t_{\rm syn} \approx 1.3 \times 10^{10} \left(\frac{B}{1\ \mu{\rm G}}\right)^{-2} \left(\frac{E}{1\ {\rm GeV}}\right)^{-1} \quad \text{years.} \tag{1}$$

So, for typical interstellar magnetic fields ($\sim 3\,\mu$G), one finds a cooling time at 100 TeV of $\sim 1.4 \times 10^4$ years. This time is longer than, but of the same order of magnitude of the age of the supernova remnants we are considering. Because of this, Mastichiadis (1996) assumed that the ambient electron spectrum is not yet affected by radiative losses. The cooling time for IC scattering on the microwave background is of the same magnitude and so IC losses will have some effect, though possibly minor, on the shape of the electron spectrum.

Hence, as a starting point we estimate the γ–ray luminosities assuming that protons and electrons are accelerated with identical power law momentum spectra extending to the same maximum momentum $p^{\rm max}$, and that these spectra have not significantly evolved. The bremsstrahlung spectrum will have the same power-law as the electron spectrum, extending to low energy so that bremsstrahlung photons eventually dominate below the π^0 peak even for very small e/p ratios. On the other hand, the inverse Compton spectrum from an E^{-2} electron spectrum will be $\sim E^{-3/2}$, which is much flatter than the π^0 and bremsstrahlung gamma ray spectra.

We next discuss the relative importance of the various processes to the gamma ray flux based on order of magnitude estimates. The crude approximations discussed below are only used for

these order of magnitude estimates, and we use exact formulae for the results we shall present later. Furthermore, in section 5 we shall make detailed fits to the gamma ray spectra which allow for the possibility of the ambient electron spectrum being steeper than the proton spectrum, either due to a different spectrum at acceleration or due to evolution of the electron spectrum.

For this estimate we approximate the total proton spectrum (integrated over the SNR) by $N(E_p) \equiv dN/dE_p = a_p E_p^{-\alpha}$ protons GeV^{-1}. For $E_\gamma \gg m_\pi c^2/2$, the gamma-ray luminosity from π^0 production is

$$L_{\pi^0}(E_\gamma) \approx c\, n \left(\sigma_{pp}^{inel} \frac{2 Z_{N\pi^0}}{\alpha}\right) \times a_p\, E_\gamma^{-\alpha}, \tag{2}$$

where σ_{pp}^{inel} is the inelastic proton–proton cross section, $\rho \approx n\, m_p$ is the average matter density sampled by the protons and $Z_{N\pi}$ is a spectrum-weighted moment of the momentum distribution of pions produced in proton-proton collisions (Gaisser 1990). For $\alpha = 2.0$, 2.3, and 2.4 respectively, $Z_{N\pi^0} \approx 0.16$, 0.075 and 0.066. Thus, for $\alpha = 2.0$

$$L_{\pi^0}(E_\gamma) \approx 1.5 \times 10^{-16}\, a_p\, n\, E_\gamma^{-2} \quad \text{photons GeV}^{-1}\ \text{s}^{-1} \tag{3}$$

where E_γ is in GeV and n is in cm^{-3}.

Similarly, we approximate the total electron spectrum by $N(E_e) \equiv dN/dE_e = a_e E_e^{-\alpha}$ electrons GeV^{-1}. To obtain the bremsstrahlung luminosity, we assume that after an electron of energy E_e has traveled one radiation length, X_0, it is converted into a photon of energy $E_\gamma = E_e$. Hence,

$$L_{\rm brem}(E_\gamma) \approx N(E_\gamma)\rho c/X_0. \tag{4}$$

Thus, for $\alpha = 2.0$,

$$L_{\rm brem}(E_\gamma) \approx 7 \times 10^{-16} a_e n E_\gamma^{-2} \quad \text{photons GeV}^{-1}\ \text{s}^{-1}. \tag{5}$$

For inverse Compton scattering, we approximate the photon energy after scattering by an electron of energy $E_e = \gamma m_e c^2$ by $\gamma^2 \bar{\varepsilon}$ where $\bar{\varepsilon}$ is the mean photon energy of the radiation field under consideration. Provided the Compton scattering is in the Thomson regime ($\gamma\bar{\varepsilon} \ll m_e c^2$) this gives an inverse Compton luminosity

$$L_{\rm IC}(E_\gamma) \approx N(\gamma) n_{\rm ph} \sigma_T c/2\gamma\bar{\varepsilon} \tag{6}$$

where $N(\gamma)d\gamma = N(E_e)dE_e$, and we obtain

$$L_{\rm IC}(E_\gamma) \approx a_e \frac{(\bar{\varepsilon})^{1/2}}{E_\gamma^{3/2}} \frac{n_{\rm ph}\sigma_T c}{m_e c^2}. \tag{7}$$

For scattering off the microwave background, we use $n_{\rm ph} = 400$ cm^{-3}, $\bar{\varepsilon} = 6.25 \times 10^{-4}$ eV, and obtain

$$L_{\rm IC}(E_\gamma) \approx 1.3 \times 10^{-14} a_e E_\gamma^{-3/2} \quad \text{photons GeV}^{-1}\ \text{s}^{-1} \tag{8}$$

where E_γ is in GeV. We note that, for an assumed matter density of 1 cm^{-3}, at 1 GeV the inverse Compton scattering contribution is an order of magnitude larger than the bremsstrahlung contribution, and the relative importance of the inverse Compton scattering contribution increases with energy. In the next two sections we describe the radiation and matter environments of the two SNR, and our accurate treatment of pion production, bremsstrahlung, and inverse Compton scattering.

3. The environments of IC 443 and γ Cygni

In addition to the microwave background radiation, and the galactic infrared/optical background radiation, the radiation produced locally within the SNR will provide target photons for inverse Compton scattering. The two SNR we consider are at galactocentric radii sufficiently close to that of the Sun that we may use the local infrared/optical radiation field for the galactic background. We adopt the spectrum of Mathis et al. (1983) which is the sum of 6 diluted blackbody spectra and is shown in Figure 1. The mean photon energy for this spectrum is $\bar{\varepsilon} \approx 0.08$ eV, and the total photon number density is $n_{\rm ph} \approx 8.6$ cm^{-3}, giving an energy density of $U_{\rm ph} \approx 0.66$ eV cm^{-3}. Using Equation 7 we can estimate the gamma ray luminosity applicable to the Thomson regime

$$L_{\rm IC}(E_\gamma) \approx 3.1 \times 10^{-15} a_e E_\gamma^{-3/2} \quad \text{photons GeV}^{-1}\ \text{s}^{-1}. \tag{9}$$

This is only a factor ~ 4 lower than that for scattering off the microwave background, and so it is necessary to include this radiation field in an accurate calculation.

Lozinskaya (1991) gives an excellent discussion of the supernova remnants IC 443 and γ Cygni. We consider first the remnant IC 443 which is at a distance of ~ 1.5 kpc, and has an angular diameter of $\sim 45'$ giving a radius of ~ 10 pc. The remnant is probably about 5000 years old and is expanding into a very inhomogeneous medium including dense molecular clouds. Most of the remnant has a temperature of $\sim 1.2 \times 10^7$ K (Petre et al 1988). Recent measurements by Asaoka and Aschenbach (1994) of the X–ray spectrum indicate two components: ~ 27 M$_\odot$ at 1 KeV, and ~ 6 M$_\odot$ at 13 KeV. Identifying the swept-up mass with 27 M$_\odot$ leads to a pre-SNR interstellar density of ~ 0.3 cm^{-3}. Petre et al. (1988) measured the X–ray flux in the 2–10 keV range, 6.7×10^{-11} erg cm^{-2} s^{-1}, and a temperature of 1.03 keV. Approximating the spectrum by a thermal bremsstrahlung spectrum, we obtain a total X–ray energy flux of 3×10^2 eV cm^{-2} s^{-1}. Dividing by the solid angle subtended by the SNR, and multiplying by $4\pi/c$ we get an approximation to the X–ray energy density in the remnant of 3×10^{-3} eV cm^{-3}. For a mean photon energy of $\bar{\varepsilon} \approx 1$ keV, one obtains a photon number density of $n_{\rm ph} \approx 10^{-6}$ cm^{-3}. Using Equation 7 we can estimate the gamma ray luminosity applicable to the Thomson regime (in this case for $E_\gamma \ll 1$ GeV)

$$L_{\rm IC}(E_\gamma) \approx 4.2 \times 10^{-20} a_e E_\gamma^{-3/2} \quad \text{photons GeV}^{-1}\ \text{s}^{-1}. \tag{10}$$

At higher energies (where scattering is in the Klein-Nishina regime) the gamma ray luminosity will be much lower. Comparing the flux from inverse Compton scattering on the X–ray emission with that from inverse Compton scattering on the microwave background, we find it to be negligible in IC 443. However, in younger supernova remnants the X–ray emission may present a significant target for IC scattering.

The supernova remnant associated with γ Cygni, G78.2+2.1, is at a distance of ~ 1.8 kpc, and has an angular size of $\sim 1^\circ$ giving a radius of ~ 16 pc. The remnant is probably about 7000 years old and is also expanding into a very inhomogeneous medium including dense molecular clouds. A dense cloud occupies $\sim 5\%$ of the volume of the remnant and this has been used by Pollock (1985) to predict the gamma ray flux (see also Aharonian, Drury, & Völk 1994). We shall return to a discussion of the effects of an inhomogeneous interstellar medium later when we discuss the electron to proton ratio. The X–ray flux obtained by Higgs, Landecker, & Seward (1983) in the 0.2–4 keV range is about 6×10^{-11} erg cm^{-2} s^{-1}, with a temperature of 1.3 keV and ambient gas density of ~ 0.2 cm^{-3}. The X-ray intensity is of the same order of magnitude as from IC 443, and so we conclude that inverse Compton scattering on the X–rays in γ Cygni, and other old SNR, will not make an important contribution to the gamma ray flux.

A major component of the radiation field of SNR is the infrared emission due to shock heated dust. For both sources, Saken, Fesen, & Shull (1992) provide infrared spectra obtained with the IRAS satellite. We use their two-temperature model fits to represent the radiation field in the infrared. We have used the solid angle subtended by each source to obtain the energy density from the intensity. In IC 443 the mean photon energies, number densities, and energy densities of the two diluted blackbody components are: $\bar{\varepsilon} \approx 0.008$, 0.04 eV; $n_{\rm ph} \approx 18.4$, 11.8 cm^{-3}; $U_{\rm ph} \approx 0.15$, 0.51 eV cm^{-3}. In γ Cygni the mean photon energies, number densities, and energy densities of the two diluted blackbody components are: $\bar{\varepsilon} \approx 0.009$, 0.025 eV; $n_{\rm ph} \approx 37.3$, 6.2 cm^{-3}; $U_{\rm ph} \approx 0.32$, 0.15 eV cm^{-3}. In both cases the infrared photon densities exceed the diffuse Galactic infrared photon densities, and so inverse Compton scattering of locally produced infrared photons could make a substantial contribution to the total inverse Compton flux. The total radiation field we adopt is shown in Fig. 2(a) for IC 443 and in Fig. 2(b) for γ Cygni, and in each case we show the contributions of the diffuse background and the locally produced radiation. The IRAS data (Saken, Fesen, & Shull 1992, Mufson et al. 1986) are also shown.

4. Accurate treatment of pion production, bremsstrahlung and inverse Compton scattering

For interactions with matter we assume standard interstellar composition. For proton interactions we use the event generator TARGET (Gaisser, Protheroe & Stanev 1983) in its proton target version. TARGET, which has been extensively tested in numerous applications, represents correctly the proton interaction cross sections and the secondary particles spectra starting at the pion production production threshold. At energies above 100 GeV the interaction cross section has

a $\ln^2 s$ behavior for proton–proton interactions. At total proton energy below 2.5 GeV TARGET generates only Δ resonances. The output of this part of the code was compared with the results of Dermer (1986) and is in good agreement.

In the case of bremsstrahlung, yields are calculated for fully ionized matter for which the cross–section is strongly energy dependent. We use the expressions of Koch & Motz (1959) with form factors for hydrogen and helium adjusted to represent the more precise values of Tsai (1974). The cross-sections for fully ionized matter are calculated with the bremsstrahlung formulae valid in the absence of screening by the atomic electrons. These cross sections are given by Protheroe, Stanev, & Berezinsky (1995).

For inverse Compton scattering we use the Klein-Nishina cross section (Jauch & Rohrlich 1976) to calculate the mean free path and the distribution of photon energies produced in the IC process. We perform an exact Monte Carlo simulation of interactions as described by Protheroe, Mastichiadis & Dermer (1992) to build up distributions of secondary electrons and photons arising from interactions of electrons of a given energy with blackbody radiation of given temperature. These distributions are then convoluted with the parent electron spectrum.

5. Results and comparison to experimental data

We assume the momentum spectrum of accelerated particles is of the form

$$\frac{dN}{dp} = ac\left(\frac{p}{1\,\mathrm{GeV/c}}\right)^{-\alpha} \quad (\mathrm{GeV/c})^{-1} \tag{11}$$

so that the energy spectrum is

$$\frac{dN}{dE} = a\left(\frac{E}{1\,\mathrm{GeV}}\right)\left(\frac{p}{1\,\mathrm{GeV/c}}\right)^{-(1+\alpha)} \quad \mathrm{GeV}^{-1} \tag{12}$$

where $E = (p^2c^2 + m^2c^4)^{1/2}$. We allow for different normalizations and spectral indices of protons (a_p, α_p) and electrons (a_e, α_e), and define the electron to proton ratio as $R_e \equiv a_e/a_p$ which is the ratio of the differential momentum spectra at 1 GeV/c. At high energies ($E \gg m_pc^2$) the energy spectrum of protons is just $dN_p/dE \approx a_pE^{-\alpha_p}$ GeV^{-1}, which gives the total number of protons per unit energy at the supernova remnant. Similarly, for electrons at high energies ($E \gg m_ec^2$) the energy spectrum is $dN_e/dE \approx a_eE^{-\alpha_e}$ GeV^{-1}.

We calculate gamma ray emissivities for π^0 production, bremsstrahlung, and inverse Compton scattering in the radiation fields appropriate to each SNR for the case where $a_p/V = 1$ GeV^{-1} cm^{-3} (V is the volume of the region where the accelerated particles are located), $R_e = 1$, and a nucleon density of $n = 1$ cm^{-3}. The emissivities are calculated for each process for a range of α for the case where $\alpha_e = \alpha_p = \alpha$, assuming $n = 1$ cm^{-3}, $R_e = 1$, and a radiation field analogous to Fig. 2a (IC 443). The emissivity, $Q(E_\gamma) \equiv dQ_\gamma/dE_\gamma$ (cm^{-3} s^{-1} GeV^{-1}), multiplied by E_γ^2, is

shown in Fig. 3 for $\alpha = 2$. With the exception of the local infrared radiation field (short dashes in Fig. 3), and neglecting the small differences of the galactic infrared background as a function of the galactocentric distance, this emissivity spectrum is universal for SNR in the Galaxy (with suitable scaling of π^0 and bremsstrahlung emissivity with matter density) on the assumption that supernova remnants accelerate charged particles with a p^{-2} spectrum, and that radiative losses have not yet affected the electron spectrum. The main feature of the emissivity spectrum is the dominance of the inverse Compton scattering (as already expected from Eq. 7) with its very flat spectrum.

It is instructive to follow the scaling of the emissivities of different processes with the supernova remnant parameters. The relative contribution of IC scales up or down only with the electron to proton ratio. In the vicinity of $E_\gamma = 1$ GeV the electron to proton ratio has to be of order of 0.01 for the IC scattering on the microwave background not to exceed the π^0 contribution for a matter density of 1 nucleon cm^{-3} and $\alpha = 2$. As long as IC is the most important contribution, the gamma-ray spectrum will be harder than the parent electron spectrum. The π^0 contribution scales only with the matter density. Alternatively, if the matter density is very high, ~ 100 nucleons cm^{-3} one can suppress the IC contribution relative to the bremsstrahlung and π^0 contributions. For such high densities, more than two orders of magnitude higher than the average densities expected from the mass of the ejecta (Lozinskaya 1991), the contribution of bremsstrahlung, which is proportional both to matter density and to the electron to proton ratio, would dominate. For a π^0 'bump' to be visible requires an electron to proton ratio less than 1.

We define Q_0^π, $Q_0^{\rm brem}$, and $Q_0^{\rm IC}$ to be the gamma ray emissivities (cm^{-3} s^{-1} GeV^{-1}) for pion production, bremsstrahlung, and inverse Compton scattering calculated for $A \equiv a_p/V = 1$ GeV^{-1} cm^{-3}, $R_e = 1$, and $n = 1$ cm^{-3}. Then the gamma ray flux observed at Earth, a distance d from the SNR, is given by

$$F_\gamma(E_\gamma, \alpha) = \frac{n_1 A_1 V}{4\pi d^2} \left[Q_0^\pi(E_\gamma, \alpha) + R_e Q_0^{\rm brem}(E_\gamma, \alpha) + \frac{R_e}{n_1} Q_0^{\rm IC}(E_\gamma, \alpha) \right] \tag{13}$$

where $n_1 \equiv n/(1\ {\rm cm}^{-3})$, n is the nucleon number density in the region of the SNR containing the accelerated particles, and $A_1 \equiv A/(1\ {\rm GeV}^{-1}\ {\rm cm}^{-3})$. We perform a maximum likelihood fit to the EGRET data (Esposito et al. 1996) for each SNR with the following free parameters: electron to proton ratio R_e, particle spectral indices (α_p, α_e), maximum energy $E^{\rm max}$ (corresponding to an exponential cutoff, i.e. $\exp(-E/E^{\rm max})$), which could also be different for protons and electrons, R_e/n_1, and the overall normalization

$$B \equiv \frac{n_1 A_1 V}{4\pi d^2} = \left(\frac{a_p}{1\ {\rm GeV}^{-1}\ {\rm cm}^{-3}} \right) \frac{n_1}{4\pi d^2} \tag{14}$$

which has units cm GeV^{-1}.

For each SNR, the γ–rays are binned in 10 energy bins, two of which give upper limits, and so the total number of data points is not sufficiently large to fit all possible parameters simultaneously. Instead we perform four different fits corresponding to the following assumptions.

Fit 1. Both protons and electrons are accelerated with power-law spectra with the same index α and to the same maximum energy of 80 TeV. The choice of $E^{\rm max}$=80 TeV is arbitrary but sufficiently high for fitting the EGRET γ–ray spectra which only extend to ∼10 GeV and for extrapolating to the Whipple limits of several hundred GeV. The assumption of a pure power law is an approximation. Non-linear effects in cosmic-ray modified shocks generally lead to some concavity in the spectra (Jones & Ellison 1991, Berezhko 1996), though the deviation from a power-law is slight for relativistic particles. For example, the proton spectrum calculated by Ellison (1993) steepens by less than 2 per cent in the spectral index below 1 TeV from its flattest high energy value.

Fit 2. Protons and electrons are accelerated with the same spectral index α but the electron spectrum cuts off at an energy $E_e^{\rm max}$ which is a fit parameter. $E_p^{\rm max} = 80$ TeV.

Fit 3. Protons and electrons are accelerated to different power law spectra with indices α_p and α_e. The maximum acceleration energy for electrons is 1000 GeV. $E_p^{\rm max} = 80$ TeV.

Fit 4. Protons and electrons are accelerated to identical power law spectra and both cut off at the same maximum energy $E^{\rm max}$.

The fitting procedure actually consisted of a tabulation of the maximum likelihood value L for a pre–determined set of parameter values. Except for the spectral indices α which were taken on a 0.05 grid, all other parameters were introduced on logarithmic scales of $10^{0.1}$, i.e. ten parameter values per decade. This grid for the trial parameters is small enough to produce neighboring spectra well within the uncertainties of the measurements. The parameter set with a maximum L value was taken to be the best fit.

5.1. Results from Fit 1

Fig. 4 shows the fitted spectrum for the supernova remnant IC 443 in Fit 1. The upper limits on the VHE γ rays from IC 443 obtained by the Whipple observatory (Buckley et al. 1997) and from the HEGRA array (Prosch et al. 1995) are also shown in Fig. 4, and seen to be consistent with the fit, even though they were not used in the fit.

The fit gives $\alpha = 2.32\pm^{0.14}_{0.11}$. The errors are calculated from the values of α at which $\ln L = \ln L_0 - s^2/2$, where L_0 is the best fit value of the likelihood function L, and s is the number of standard deviations ($s = 1$ to give 1σ errors). The overall normalization gives $B = 4.0 \times 10^8$ cm GeV^{-1}. The electron to proton ratio corresponding to this value of α is $R_e = 0.16\pm^{0.29}_{0.08}$. The best fit value of R_e/n_1 is $\sim 10^{-4}$, with very large error bars because the emission is dominated by π^0 production and bremsstrahlung. Thus, we can not reliably give the matter density since the fit requires a very high density only to make the IC component negligible. This also prevents us from obtaining a reliable estimate of the cosmic ray density at the source.

Fig. 5 shows a similar fit for γ Cygni. The best α value is $\alpha = 2.42\pm^{0.09}_{0.07}$, which gives an

electron to proton ratio of $R_e = 0.16\pm^{0.14}_{0.08}$, and a similar value of R_e/n_1 to IC 443. The overall normalization gives $B = 10^9$ cm GeV^{-1}. The VHE limits are from Whipple (Buckley et al. 1997) and from HEGRA (Prosch et al. 1996, Willmer et al. 1995) and are again consistent with the fit.

We can get some useful information from the overall normalization constant $B \equiv n_1 A_1 V/4\pi d^2$ which, given that we know d, gives us the product of n, $N_p(p = 1 \text{ GeV/c})/V$, and V. The total energy content of a spectrum of the form of Equation 11 with $\alpha = 2.32$ and $a_p = 1$ is ~ 3 GeV. Thus for IC 443 at a distance of 1.5 kpc the normalization $B = 4.0 \times 10^8$ cm GeV^{-1} requires a total energy in accelerated protons of

$$U_{\rm CR} \sim 5 \times 10^{50} \left(\frac{n}{1 \text{ cm}^{-3}}\right)^{-1} \quad \text{erg}, \tag{15}$$

where n is the number density of gas in the region where the accelerated particles are located. The corresponding value for γ Cygni is a factor of 3 higher. Alternatively, we can obtain an estimate of the total mass in the region where the accelerated particles are located as a function of the energy density in accelerated particles

$$M \sim 3 \times 10^5 \left(\frac{u_{\rm CR}}{1 \text{ eV cm}^{-3}}\right)^{-1} \quad \text{M}_\odot \tag{16}$$

for IC 443 and a factor 3 higher for γ Cygni.

Fit 1 requires a very high matter density in order to suppress the IC contribution to the γ–ray flux which is much flatter than the observed spectrum. The SNR G78.2+2.1 associated with γ Cygni was tentatively identified with the COS-B source 2CG78+01 (Pollock et al. 1985). A cloud of density ~ 300 cm^{-3} occupies $\sim 5\%$ of the volume of the remnant, and this density has been used by Pollock (1985) in predicting GeV gamma ray fluxes. Aharonian, Drury, & Völk (1994) also discussed this association and point out that the emission may extend to TeV energies. At radio frequencies, most of the emission comes from the SE part of the remnant (Higgs, Landecker, & Roger 1983), and this appears to coincide also with a region of exceptionally high 90 μm intensity, and a molecular cloud near the rim of the remnant, implying that this region may be the source of the gamma ray emission. A density of ~ 300 cm^{-3} is comparable with the densities that come from the maximum likelihood fits. However, the fitted density is the density averaged over the region where the accelerated particles are located, and so this value may be unrealistically high unless acceleration is taking place only close to such a massive high-density cloud. This might occur at massive clouds interacting with the SNR shock.

Another way to look at the numbers for γ Cygni is to note that the energy in cosmic rays required in a region with density 300 cm^{-3} is 5×10^{48} erg. If this high density occupies 5% of the volume of the SNR then the total energy in cosmic rays, assuming them to be uniformly distributed, is $\sim 10^{50}$ erg, approximately 10% of the initial kinetic energy of the ejecta of a typical supernova.

Finally, we check that for the fitted electron spectra the synchrotron X–ray flux predicted for reasonable magnetic fields does not exceed that observed. This is particularly important for the

case of Fit 1 where the electron spectrum extends up to 80 TeV and one would expect to generate a significant X–ray flux for any standard value of magnetic field at the shock.

Taking the electron spectrum in the source to be

$$N(E) \equiv \frac{dN}{dE} = a_e E^{-\alpha} \exp(-E/E_e^{\max}) \quad \mathrm{GeV}^{-1}, \tag{17}$$

where E is in GeV, we may obtain the synchrotron X–ray flux at Earth (erg cm^{-2}) in the energy range ϵ_1 to ϵ_2

$$F_X = \frac{a_e}{4\pi d^2} \int_{\epsilon_1/h}^{\epsilon_2/h} d\nu \int dE E^{-\alpha} P(\nu, E, H_\perp). \tag{18}$$

Here $P(\nu, E, H_\perp)$ is the power per unit frequency (erg Hz^{-1}) emitted at frequency ν by an electron of energy E (GeV) in a magnetic field with perpendicular component $H_\perp$ (gauss) and is given by

$$P(\nu, E, H_\perp) = 4\pi c_3 H_\perp F(x) \tag{19}$$

where $c_3 = 1.87 \times 10^{-23}$, $x = \nu/\nu_c$, $\nu_c \approx c_1 H_\perp (625E)^2$, $c_1 = 6.27 \times 10^{18}$, and

$$F(x) = x \int_x^\infty K_{5/3}(z) dz \tag{20}$$

where $K_{5/3}$ is a Bessel function of the second kind (Pacholczyk 1970). ¿From Eq. 14 we see that

$$a_e = \frac{BR_e}{n} 4\pi d^2, \tag{21}$$

and so we obtain

$$F_X = 4\pi c_3 H_\perp \frac{BR_e}{n} \int_{\epsilon_1/h}^{\epsilon_2/h} d\nu \int dE F(x) E^{-\alpha} \exp(-E/E_e^{\max}). \tag{22}$$

For the best fit parameters given above, and a perpendicular component of magnetic field of $H_\perp = 6\mu$G, we predict for IC 443 a 2—10 keV flux of 6.8×10^{-13} erg cm^{-2} s^{-1} which is not in conflict with the observed flux of 6.7×10^{-11} erg cm^{-2} s^{-1}. Similarly for γ Cygni we predict a 0.2—4 keV flux of 8.2×10^{-12} erg cm^{-2} s^{-1} which is not in conflict with the observed flux of 6×10^{-11} erg cm^{-2} s^{-1}.

5.2. Results from Fits 2, 3, and 4

As noted above, the X-ray luminosity calculated using a magnetic field of 6 μG and the electron spectra from Fit 1 is not in direct contradiction with the observed luminosities of either object. However, for higher magnetic fields, e.g. due to shock compression, the predicted luminosity would exceed that observed if $H_\perp$ is higher than $\sim 54\mu$G (IC 443) or $\sim 42\mu$G (γ Cygni). Even for fields below these limits, there may be a problem due to the power-law nature of the

synchrotron spectrum given that the observed X–ray spectrum appears to be consistent with thermal bremsstrahlung origin.

We therefore perform Fits 2, 3, and 4, which tend to suppress the X–ray production either by cutting off the electron spectrum at an arbitrary $E_e^{\max}$ or by allowing a steeper electron spectrum. Tables I and II list the results of all four fits for the two supernova remnants. Columns 2 & 3 give the proton and electron acceleration spectra, column 4 – the cutoff energy for electrons (and protons in Fit 4), column 5 contains the preferred R_e value, column 6 – the matter density. Column 7 gives the measure of the fit improvement ($\ln(L/L_0)$) and column 8 – the maximum value of the magnetic field allowed by the observed X–ray luminosity of the source. Note that the synchrotron X–ray flux does not scale simply as a power-law in magnetic field (with exponent related the electron spectral index) because the X–ray emitting electrons are near or above $E_e^{\max}$ where the spectrum is affected by the exponential cut-off so that the delta-function approximation to $F(x)$ which is often used breaks down.

Fit 2 ($\alpha_e = \alpha_p$, $E_e^{\max}$ fitted) is not very sensitive to the spectral index at acceleration, but is quite sensitive to the cutoff energy of the electrons. Fit prefers a low value of the electron cutoff energy $E_e^{\max}$, which eliminates the problem with the flat IC γ–ray spectrum and thus does not require very large matter density. Within 1σ of the best fit values the matter density only varies by a factor of 2. Because of the low electron energy cutoff the fit allows for significantly flatter acceleration spectra. The range of R_e is significantly wider with R_e decreasing from $\sim$1 for flat spectra to $\sim$0.1 for spectral indices 1.35 – 1.40. The fit quality improves over Fit 1, especially for γ Cygni. Adding one more parameter to the fit increases the error bars on all parameters that we evaluate. The best fit spectrum for IC 443 is shown in Fig. 6.

Fit 3 (α_p, α_e fitted, $E_e^{\max}$ fixed) also allows for a wide range of spectral indices. The most important restriction that data requires is an electron acceleration spectrum which is significantly steeper than the proton spectrum. Even these steep electron spectra do not fully compensate for the flat IC production spectrum, so that the matter density required is of order 1–10 cm^{-3}. The R_e value is quite stable, $\sim$0.1–0.2 or even less for IC 443. The fit quality improves over Fit 1 by more than 1σ for both supernova remnants. Fig. 7 shows the best fit spectrum for IC 443 under

Table 1: Fit parameters for IC 443. $E_p^{\max}$ fixed at 80 TeV for fits 1, 2 & 3. $E_e^{\max}$ fixed at 80 TeV for fit 1 and at 1 TeV in fit 3.

Fit	α_p	α_e	$E_e^{\max}$ (GeV)	R_e	n (cm^{-3})	$\ln(L/L_0)$	$H_\perp^{\max}$ (G)
1	$2.32^{+0.14}_{-0.11}$	$=\alpha_p$	8×10^4	$0.16^{+0.29}_{-0.08}$	$>10^3$	0	5.4×10^{-5}
2	$2.15^{+0.15}_{-0.15}$	$=\alpha_p$	25^{+15}_{-10}	$0.4^{+2.0}_{-0.3}$	$0.6^{+0.4}_{-0.2}$	0.36	7.0×10^{-2}
3	$2.25^{+0.20}_{-0.20}$	$2.70^{+0.15}_{-0.35}$	10^3	$0.05^{+0.15}_{-0.02}$	$6.3^{+10.}_{-5.0}$	0.68	5.3×10^{-4}
4	$1.85^{+0.30}_{-0.15}$	$=\alpha_p$	40^{+23}_{-24}	$0.03^{+0.07}_{-0.02}$	$0.08^{+0.12}_{-0.02}$	1.22	1.2×10^{-2}

the assumptions of Fit 3.

Fit 4 ($\alpha_e = \alpha_p$, $E_p^{\max} = E_e^{\max}$ fitted) produces the greatest improvement for both objects. This is especially true for γ Cygni, for which all three previous sets of assumptions give significantly worse fits. Fig. 8 shows the best fit spectrum for γ Cygni. It is important to notice that the contribution of the individual processes is now different. The role of bremsstrahlung is negligible. The γ–ray fluxes above 1 GeV are due to π^0 production while IC dominates at lower energy. The power law spectra preferred by the fits are very flat (α <2), R_e <0.1, and the matter density is less than 0.1. Both electron and proton spectra cut off at less than 60 GeV.

6. Conclusions

With the current set of assumptions the fits of the γ–ray spectra of the two supernova remnants identified three possible sets of basic parameters. The first set, represented by Fit 1, consists of a relatively steep acceleration spectra and requires very large matter density in the acceleration region. The second set, Fits 2 & 3 allows for more reasonable matter densities at the γ–ray production region. Fit 4, which assumes a cutoff of the electron and proton spectra at the same maximum energy, results in a low matter density but also a very low value of the maximum energy. A fit with E_p^{max} allowed to increase while keeping E_e^{max} low would give a similar fit to the EGRET data, but steepening the electron spectrum through synchrotron radiation at such a low energy would require extreme magnetic fields.

Note that recent theoretical calculations, accounting for nonlinear effects (Berezhko 1996; Ellison & Reynolds 1991), predict compression ratios higher than 4 that could lead to mean slopes at acceleration much flatter than the canonical $\alpha = 2$ value. Flat electron spectra at low energies would also be more consistent with the radio spectral indices of the two supernova remnants which imply electron spectral indices at low energies of $\alpha_e = 1.72$ for IC443, and $\alpha_e = 2.0$ for γ Cyg (Green 1991). Fits 1 to 3 (IC 443) and Fits 1 and 3 (γ Cygni) appear to be inconsistent with the radio data. However, if a high magnetic field were present (i.e. close to $H_\perp^{\max}$) then the energies of

Table 2: Fit parameters for γ Cygni. $E_p^{\max}$ fixed at 80 TeV for fits 1, 2 & 3. $E_e^{\max}$ fixed at 80 TeV for fit 1 and at 1 TeV in fit 3.

Fit	α_p	α_e	$E_e^{\max}$ (GeV)	R_e	n (cm^{-3})	$\ln(L/L_0)$	$H_\perp^{\max}$ (G)
1	$2.42^{+0.09}_{-0.07}$	$= \alpha_p$	$[8 \times 10^4]$	$0.16^{+0.29}_{-0.08}$	$> 10^3$	0	4.2×10^{-5}
2	$2.25^{+0.15}_{-0.25}$	$= \alpha_p$	25^{+15}_{-10}	$0.50^{+0.50}_{-0.40}$	$4.0^{+2.3}_{-2.7}$	1.07	6.6×10^{-3}
3	$2.35^{+0.10}_{-0.20}$	$2.50^{+0.20}_{-0.10}$	$[10^3]$	$0.13^{+0.20}_{-0.03}$	$12.0^{+7.}_{-4.}$	0.81	7.8×10^{-5}
4	$1.80^{+0.10}_{-0.15}$	$= \alpha_p$	40^{+23}_{-5}	$0.04^{+0.06}_{-0.03}$	$0.06^{+0.04}_{-0.03}$	5.57	1.7×10^{-3}

the electrons producing the radio synchrotron emission could be much lower than the energies of the γ-ray emitting electrons, thereby removing the inconsistency. This would occur, for example in the case of Fit 2, where the synchrotron emitting electrons could have energies as low as 5 MeV (IC 443).

The improvement of fit quality, shown in Tables 1 and 2, increases as expected when an additional fit parameter is introduced. We have not employed the F–test, which measures the fit improvement with the increase of number of parameters, because our different fits do not correspond to particular models of supernova remnants that we are testing. It is important to notice that $\ln(L/L_0)$ value is to a large extent determined by the end points of the data set where the efficiency and the statistical accuracy of the EGRET measurements are the worst.

Following the EGRET observation of IC 443 and γ Cygni it was anticipated, based on an E^{-2} extrapolation of the observed flux, that these sources should be observable in the TeV range and above with ground based detectors. A simple E^{-2} extrapolation of the Egret data is inconsistent with upper limits from CASA (Borione et al. 1995) and Cygnus (Allen et al. 1995) around 100 TeV, from Hegra above 20 TeV and from Whipple above 300 GeV. In this context, it is interesting to note that, except for Fit 4, which has very low E^{max}, our fits to the EGRET data alone seem to indicate steeper source spectra.

The upper limits of the Whipple observatory on the TeV emission from the sources is shown on all emission spectra shown in Figs. 4 – 8. It is important to notice that the fitted spectra are always below, or very close to, the experimental upper limits. In the case of Fit 1 of IC 443 (Fig. 4), for example, the fitted spectrum is $\sim$50% higher than the upper limit. Half of that difference is due to the contribution of bremsstrahlung. Note however, that if the interactions are taking place with neutral matter, such as that in a molecular cloud, then the cross sections we have used for bremsstrahlung in ionized matter would be inappropriate, and the bremsstrahlung spectral index could be steepened by as much as ~ 0.1 which would have the effect of bringing the fitted spectrum below the experimental limit.

An electron source spectrum with $\alpha \sim 2.4$ is favored by a comparison of recent cosmic ray electron propagation calculations with direct cosmic ray electron observations above $\sim$ 10 GeV (Strong et al. 1994, Strong & Youssefi 1995, Porter & Protheroe 1997). However, source spectra as flat as E^{-2} are possible (Aharonian, Atoyan, & Völk 1995) if the distance to the nearest source is $\sim$ 100 pc or more. The spectra of the two SNR observed by EGRET show no sign of flattening at, or below, 100 MeV, indicating the presence of a steep spectral component due to bremsstrahlung.

There are many different implications of a steep spectrum on acceleration ($\alpha \sim 2.2 - 2.4$), extracted with some of the assumptions of our analysis (Fits 1–3). For example, such a source spectrum for cosmic ray nuclei would require a loss rate in the galaxy, and hence a diffusion coefficient for cosmic ray propagation, proportional to $\sim E^{0.3}$ rather than $\sim E^{0.7}$ which is usually assumed based on cosmic ray secondary to primary ratios (note that a Kolmogorov spectrum actually predicts a diffusion coefficient proportional to $E^{1/3}$, see also Ptuskin et al. 1993, and

Biermann 1995). Such a diffusion coefficient is also favored by reacceleration models (Heinbach & Simon 1995, Seo & Ptuskin 1994). Such spectra, however, would not be consistent with the radio observations and would require a strong spectral steepening above radio emitting energies.

In conclusion, we have modeled the gamma ray emission of IC 443 and γ Cygni including inverse Compton scattering on all relevant radiation fields, bremsstrahlung, and pion production. We fit the modeled production spectra to the EGRET data assuming a power-law momentum spectrum of electrons and nuclei in the SNR and exponential cutoffs. The results from the fitting show that (a) the dominant contributions come from bremsstrahlung and π^0 decay provided the spectra of both electrons and nuclei extend above 60 GeV. The IC contribution can only be important with fine tuning, when $E^{\rm max}$ for both electrons and nucleons is $\sim$40 GeV; (b) an electron to proton ratio of $\sim$ 0.05–0.5 is required under all four assumptions that we have explored; (c) a spectral index of $\alpha \sim 2.2$–2.4 is required if electrons and nuclei are accelerated with the same spectral indices unless the acceleration spectra cut off below 60 GeV; (d) if the acceleration spectra of electrons and nuclei are not the same the data requires electron spectra that are significantly steeper than the nuclei spectra, which contribute to the experimentally observed range only the π^0 feature, which depends mildly on the acceleration spectra of nuclei; (e) a very high, but uncertain, average matter density is required if the electron spectrum has the same spectral index as the proton spectrum and the cut-off energy is very high, e.g. 80 TeV (note, however, that matter densities as high as $\sim$ 300 cm^{-3} are present in molecular clouds associated with these SNR). We also note that in this case the bremsstrahlung contribution at 1 GeV is $\sim$ 40%, somewhat higher than the $\sim$ 10% obtained from a fit to the diffuse galactic gamma ray intensity (Hunter et al. 1995, Hunter et al. 1997), which is probably lower due to the effects of cosmic ray energy losses during propagation which are different for electrons and nuclei.

At the present time and with the current available experimental information we cannot make a choice between the two basic assumptions that we used for fitting the EGRET data. Additional experimental information is necessary for further analysis. One crucial data set would consist of TeV detections (or lower upper limits) of these two and other supernova remnants. A possible observation would allow us the exclude the assumption for a low energy cutoff of the acceleration spectra and to obtain better determined values for the shape of the electron and proton spectra and for the matter density at the source. We also plan to extend our analysis by using theoretically motivated shapes for the spectra of the accelerated particles. It will then be possible to also predict the expected 100 TeV γ–ray fluxes from supernova remnants in some current models (Berezhko 1996), which extend the accelerated particles spectra to Z$\times$400 TeV.

Acknowledgements. We thank Joe Esposito and the EGRET group for providing the measured spectra of IC 443 and γ Cygni in numerical form. We are grateful to the referee Steven Reynolds for helping us to improve on the first version of this paper. RJP thanks the Bartol Research Institute for hospitality during part of 1996. We thank Troy Porter for a useful discussion and for reading the manuscript. The research of TKG is supported in part by NASA Grant NAGW–4605.

TS is supported in part by NASA grant NAGW–3880. The research of RJP is supported by a grant from the Australian Research Council.

REFERENCES

Aharonian, F.A., Drury, L.O'C., Völk, H.J. 1994, A&A, 285, 645

Aharonian, F.A., Atoyan, A.M., & Völk, H.J. 1995, A&A, 294, L41

Allen, G.E., et al. 1995, ApJ, 448, L25

Asaoka, I., & Aschenbach, B. 1994 A&A, 284, 573

Berezhko, E.G., & Krymski, G.F. 1988, Usp. Fiz. Nauk, 154, 49

Berezhko, E.G. 1996, Astropart. Phys., 5, 367

Biermann, P.L. 1995, Nucl. Phys. B, S43, 221

Blandford, R, & Eichler, D. 1987, Phys. Rep., 154, 1

Borione, A., et al. 1995, Proc. 24th Int. Cosmic Ray Conf. (Rome), vol. 2, p. 439

Buckley, J.H. *et al.* 1997, A&A, submitted

Dermer, C.D. 1986, A&A, 157, 223

Drury, L.O'C. 1983, Space Sci. Rev., 36, 57

Drury, L.O'C., Aharonian, F.A., Völk, H.J., 1994 A&A, 287, 959

Ellison, D.C. 1993, Proc. 23th Int. Cosmic Ray Conf. (Calgary), vol. 2, p. 219

Ellison, D.C. & Reynolds, S.P. 1991 ApJ, 283, 242.

Esposito, J.A., Hunter, S.D., Kanbach, G., & Sreekumar, P., 1996 ApJ, 461, 820

Gaisser, T.K. *Cosmic Rays and Particle Physics*, Cambridge University Press.

Gaisser, T.K., Protheroe, R.J., & Stanev, T. 1983, in Proc. 18th Int. Cosmic Ray Conf. (Bangalore), Vol. 5, p. 174. (Fig. 1 in this reference is incorrectly plotted.)

Green, D.A. 1991, PASP, 103, 209.

Heinbach, U., & Simon, M. 1995, ApJ, 441, 209

Higgs, L.A., Landecker, T.L., & Seward, F.D. 1983, in "Supernova Remnants and their X–ray Emission", eds. J. Danziger & P. Gorenstein, (IAU Symp. 101), p. 281

Higgs, L.A., Landecker, T.L., & Roger, R.S. 1983,AJ, 88, 98

Hunter, S.D. et al. (EGRET team) 1995, Proc. 24th Int. Cosmic Ray Conf. (Rome), vol. 2, p. 182

Hunter, S.D. et al. 1997, ApJ, in print.

Jauch J.M., Rohrlich F. 1976, "The Theory of Photons and Electrons" (Springer-Verlag, New York)

Jones, F.C., & Ellison, D.C. 1991, Space Sci. Rev., 58, 259

Koch, H.W. & Motz, J.W. 1959, Rev. Mod. Phys., 31, 920

Koyama, K., Petre, R., Gotthelf, E.V., Hwang, U., Matsuura, M., Ozaki, M., & Holt, S.S. 1995, Nature, 378, 255

Lozinskaya, T.A. 1991, "Supernovae and Stellar Wind in the Interstellar Medium", (American Inst of Physics, New York)

Mastichiadis, A., 1996 A&A, 305, 53

Mathis, J.S., Mezger, P.G., & Panangia, N. 1983, A&A, 128, 212

Mufson, S.L., McCollough, M.L., Dickel, J.R., Petre, R., White, R. 1986, AJ, 92, 1349

Pacholczyk, A.G., 1970, "Radio Astrophysics", W.H. Freeman and Co., San Francisco.

Petre, R., Szymkowiak, A.E., Seward, F.D., & Willingale, R. 1988, ApJ, 335, 215

Pohl, M. 1996, A&A, 307, 57

Pollock, A.M.T. 1985, A&A, 150, 339

Pollock, A.M.T., et al. 1985, A&A, 146, 352

Porter, T.A., & Protheroe, R.J. 1997, J. Phys. G: Nucl. Part. Phys., in press

Prosch, C., et al. 1995, Proc. 24th Int. Cosmic Ray Conf. (Rome), vol. 2, p. 405

Prosch, C., et al. 1996, A&A, 314, 275

Protheroe, R.J., Stanev, T., & Berezinsky, V.S. 1995, Phys. Rev. D, 151, 4134

Protheroe R.J., Mastichiadis, A. & Dermer, C.D. 1992, Astroparticle Physics, 1, 113

Ptuskin, V. S., Rogovaya, S. I., Zirakashvili, V. N., Chuvilgin, L. G., Khristiansen, G. B., Klepach, E. G., & Kulikov, G. V. 1993, A&A, 268, 726

Reynolds, S.P. 1996, ApJ, 459, L13

Saken, J.M., Fesen, R.A., & Shull, J.M. 1992, ApJS, 81, 715

Seo, E.S. & Ptuskin, V.S. 1994, ApJ, 431, 705

Strong, A.W., et al. 1994, A&A, 292, 82

Strong, A,W., & Youssefi, G. 1995, Proc. 24th Int. Cosmic Ray Conf. (Rome), vol. 3, p. 48

Tsai, Y.S. 1974, Rev. Mod. Phys., 46, 815

Willmer, M., et al. 1995, Proc. 24th Int. Cosmic Ray Conf. (Rome), vol. 2, p. 409

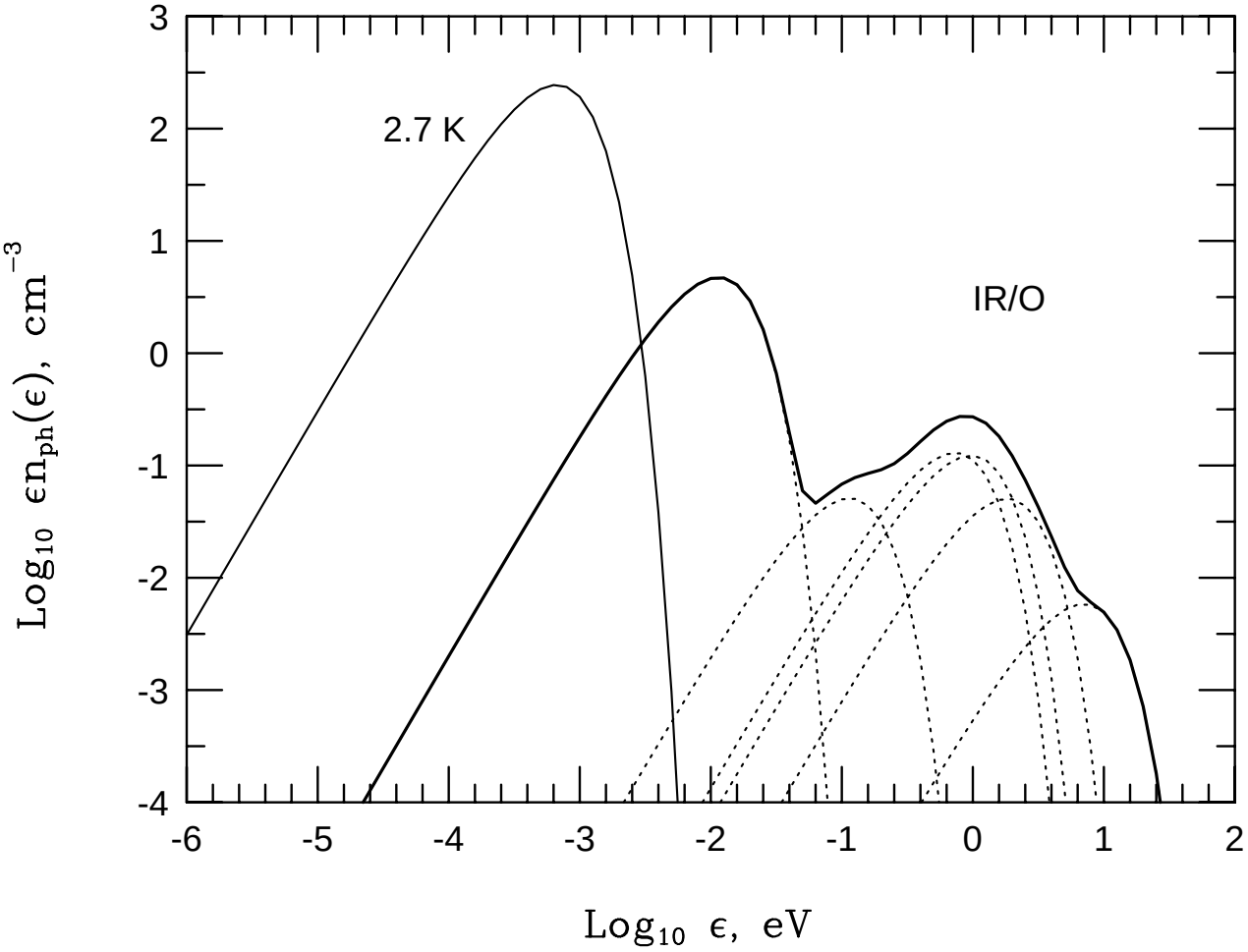

Fig. 1.— The interstellar infrared/optical (IR/O) radiation field based on the work of Mathis, Mezger, & Panangia (1983) composed of six diluted blackbody spectra (dotted lines), and the cosmic microwave background (2.7 K).

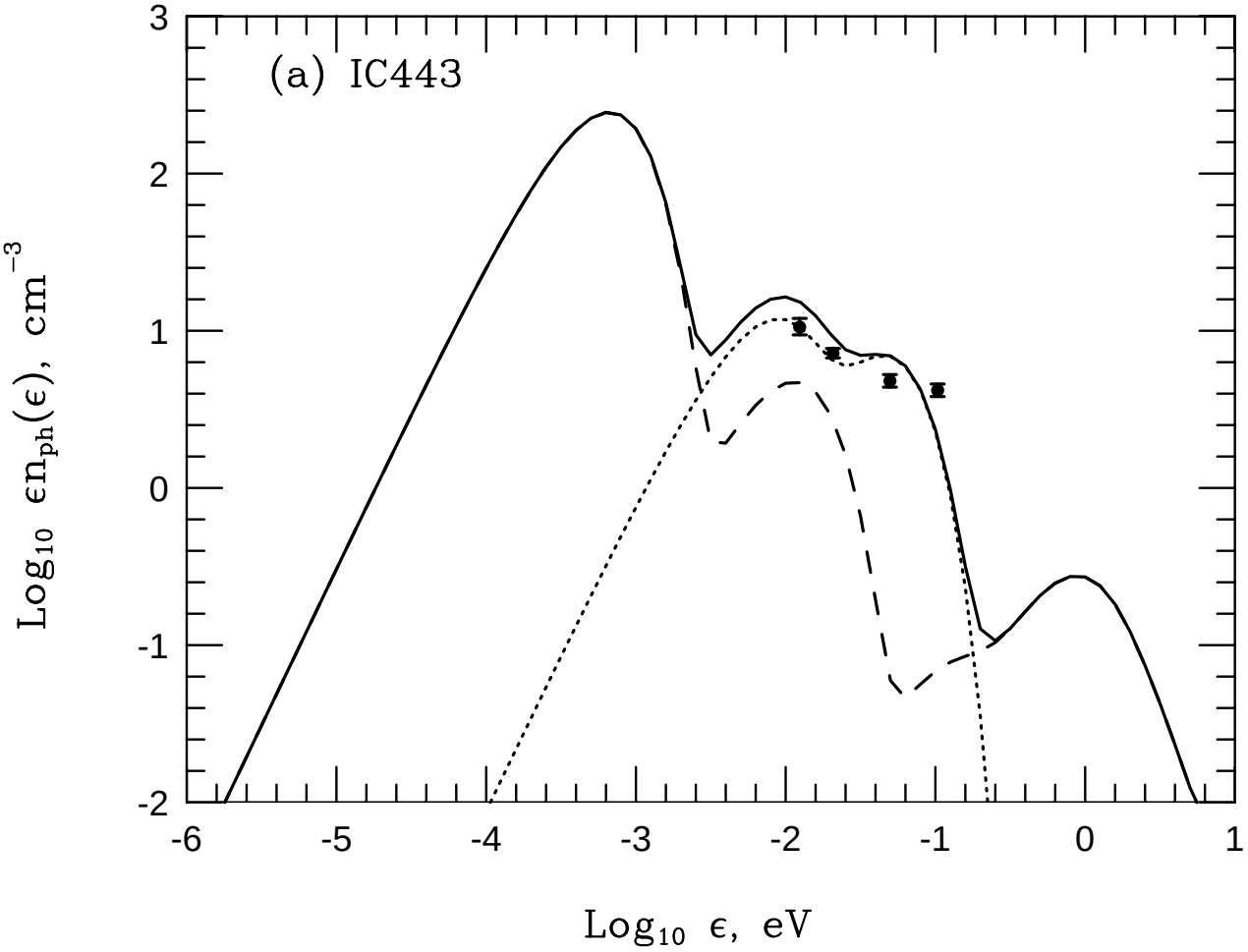

Fig. 2.— Total radiation field at the supernova remnant (solid curve) showing contributions from interstellar infrared/optical plus microwave (dashed line) and two-temperature fit to infrared spectra (Saken, Fesen, & Shull 1992) (dotted curve) and recent data for (a) IC 443 (data from Mufson et al. 1986) and (b) γ Cygni (data from Saken, Fesen, & Shull 1992).

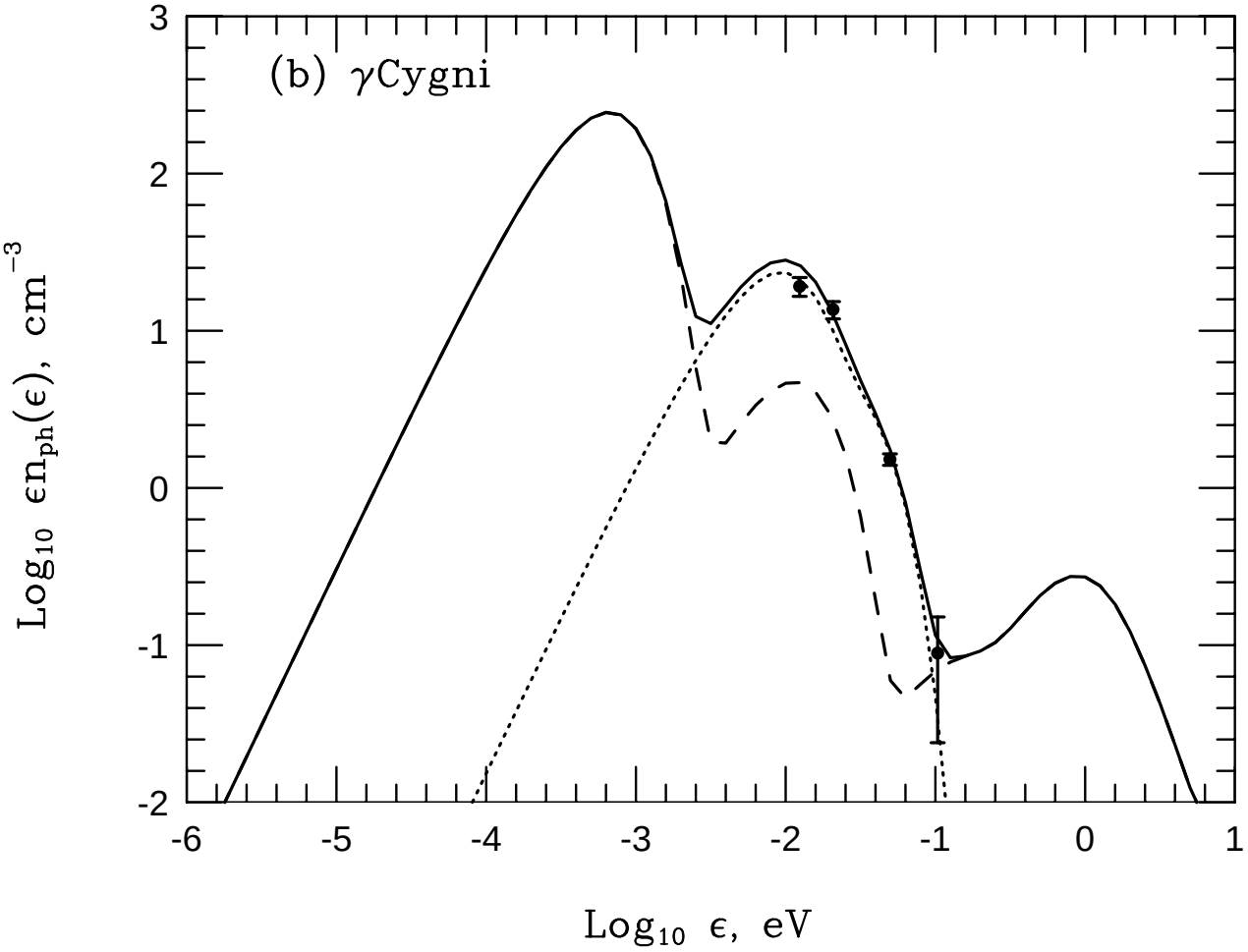

Fig. 2.— (b)

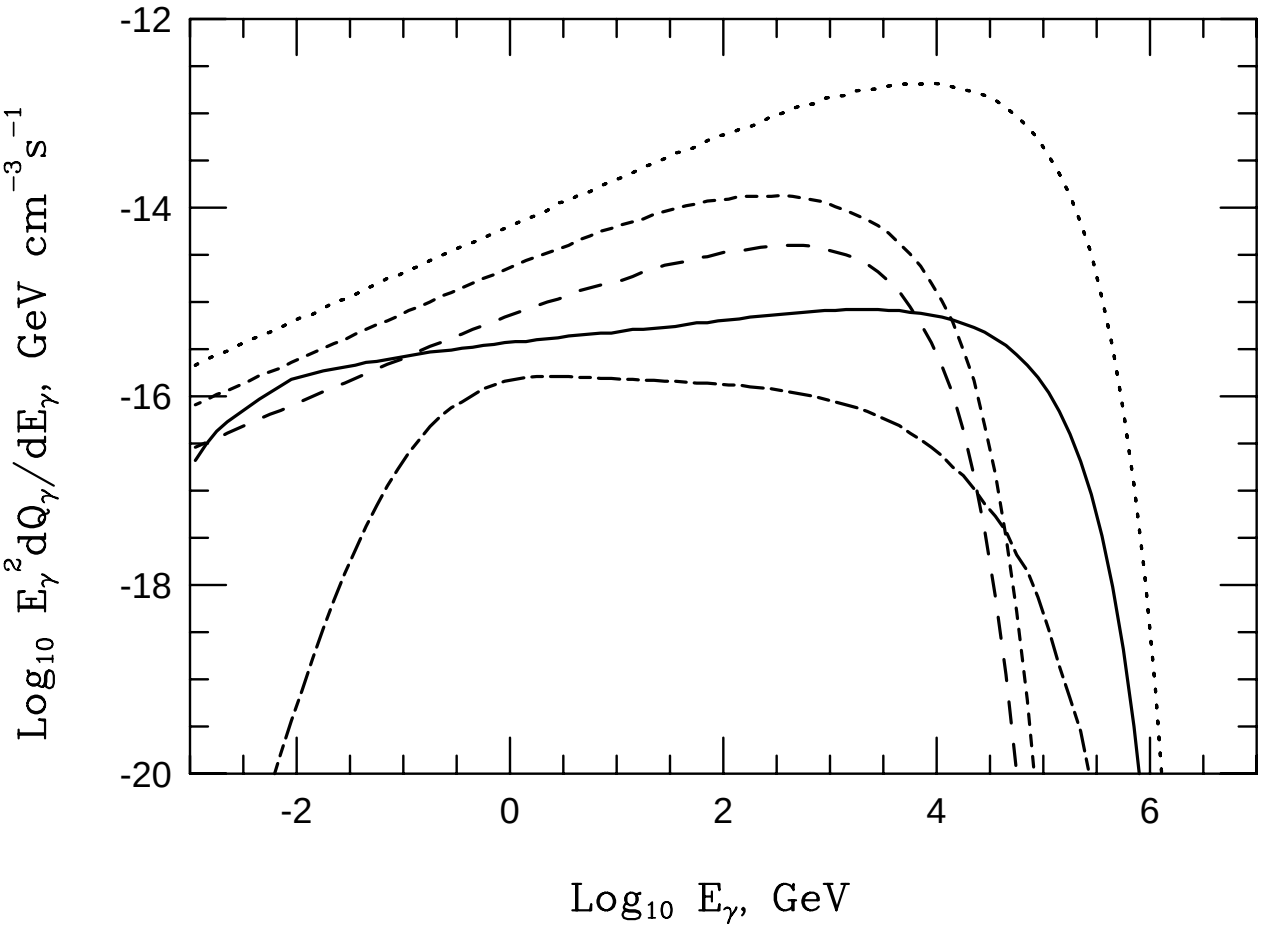

Fig. 3.— Gamma ray emissivity at IC 443 produced by particles (electrons and protons) with momentum spectrum $dn/dp = p^{-2}$ cm^{-3} GeV/c^{-1} interacting with interstellar matter with nucleon number density 1 cm^{-3} and with interstellar (IR/O) and cosmic microwave radiation fields of Figure 1: dot-dash curve – π^0 production; solid curve – bremsstrahlung; long dashes – inverse Compton on interstellar (IR/O); short dashes – inverse Compton on Infrared radiation at IC 443; dotted curve – inverse Compton on microwave.

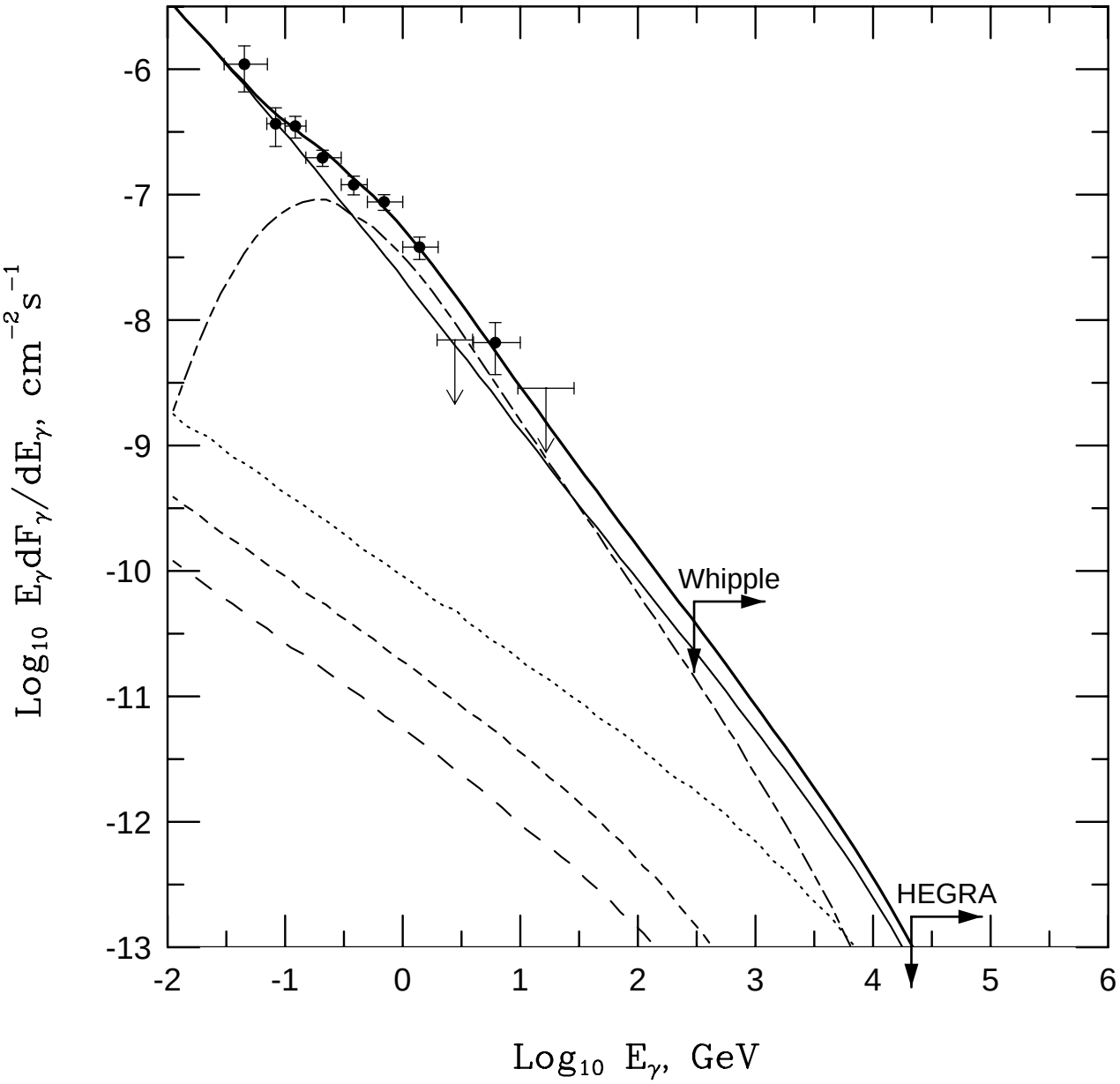

Fig. 4.— Best fit (Fit 1) to EGRET observations of IC 443, including upper limits (thick solid curve). Whipple (Buckley et al. 1997) and HEGRA upper limits (Prosch et al. 1995) are not included in the fits. The small IC contributions from the interstellar and source IR radiation are not shown in this and other fit spectra. The other curves have the same meaning as in Fig. 3.

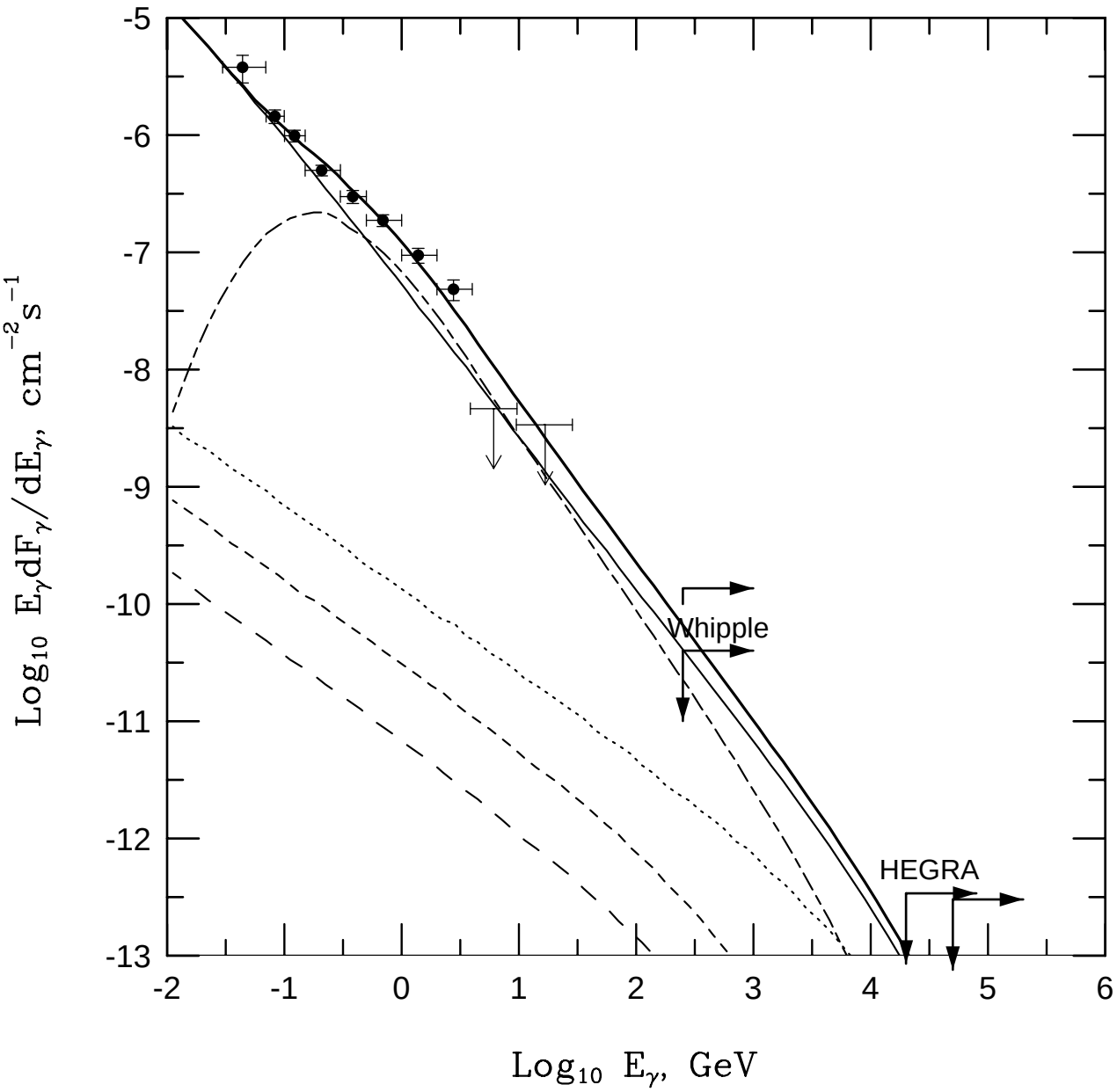

Fig. 5.— Best fit (Fit 1) to EGRET observations of γ Cygni, including upper limits (thick solid curve). Whipple (Buckley et al. 1997) and HEGRA upper limits (Prosch et al. 1996, Willmer et al. 1995) are not included in the fits.

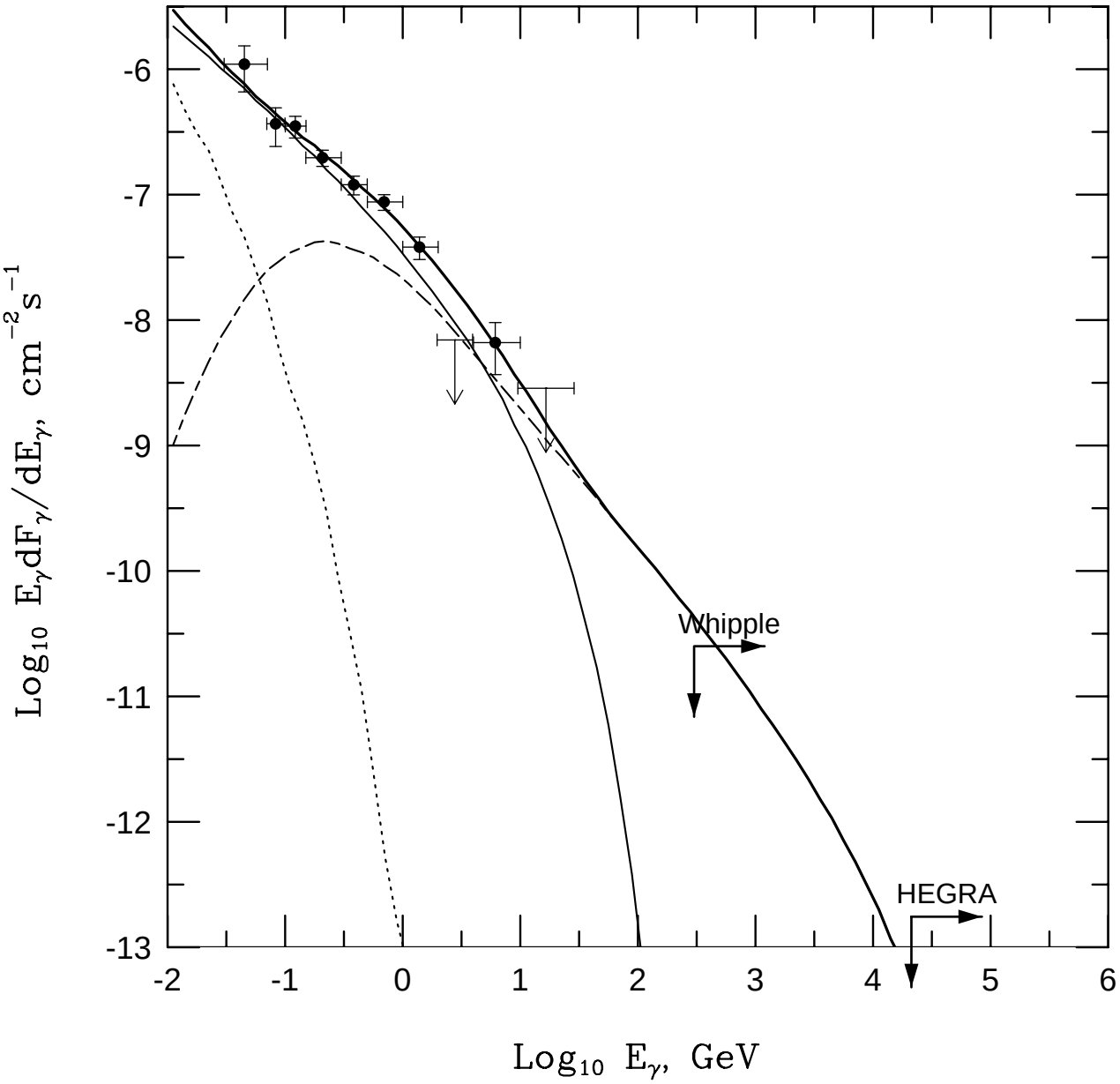

Fig. 6.— Best fit (Fit 2) of IC 443.

Gaisser, Protheroe & Stanev, Fig. 6, IC443 Fit 2

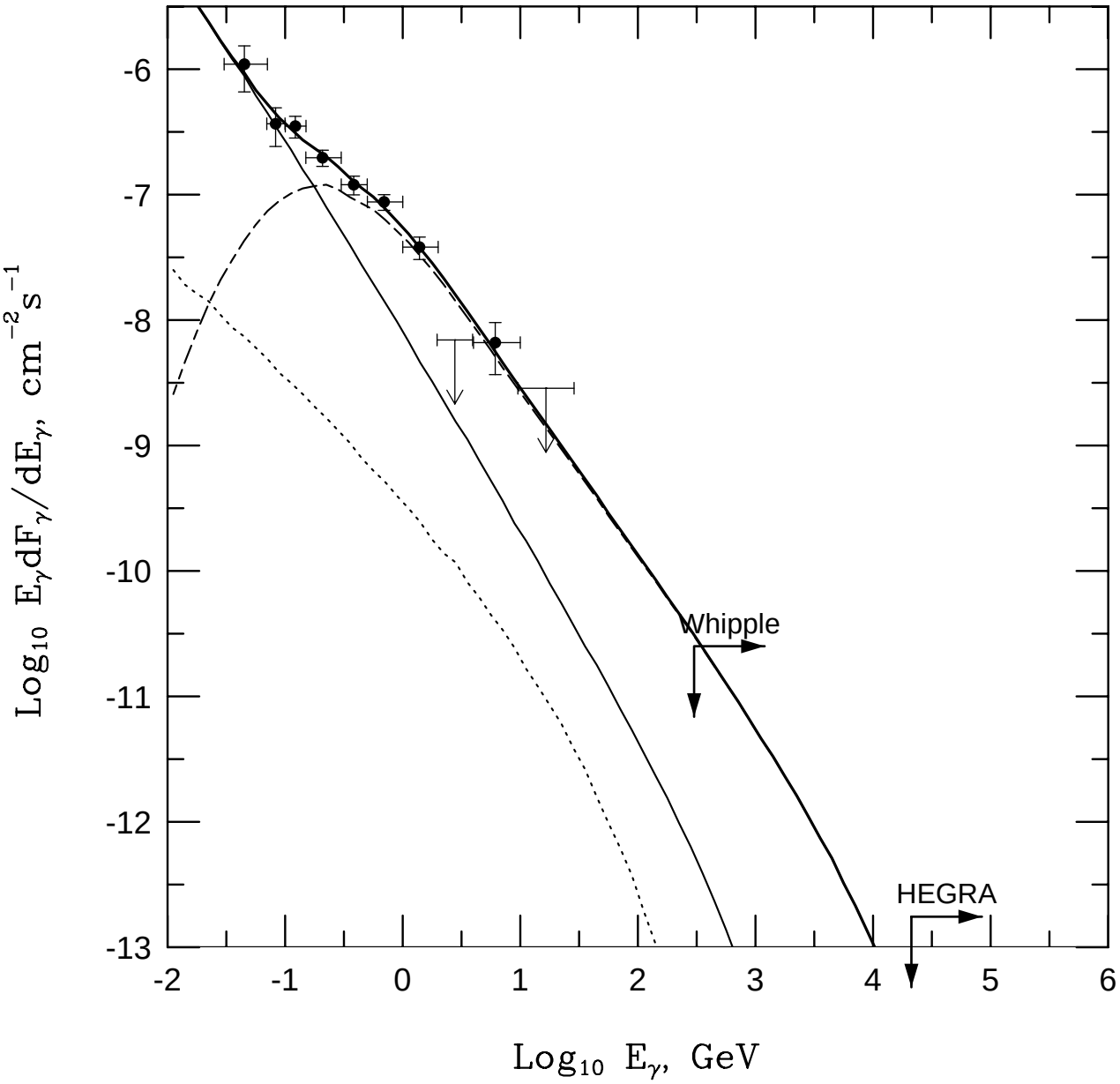

Fig. 7.— Best fit (Fit 3) of IC 443.

Gaisser, Protheroe & Stanev, Fig. 7, IC443 Fit 3

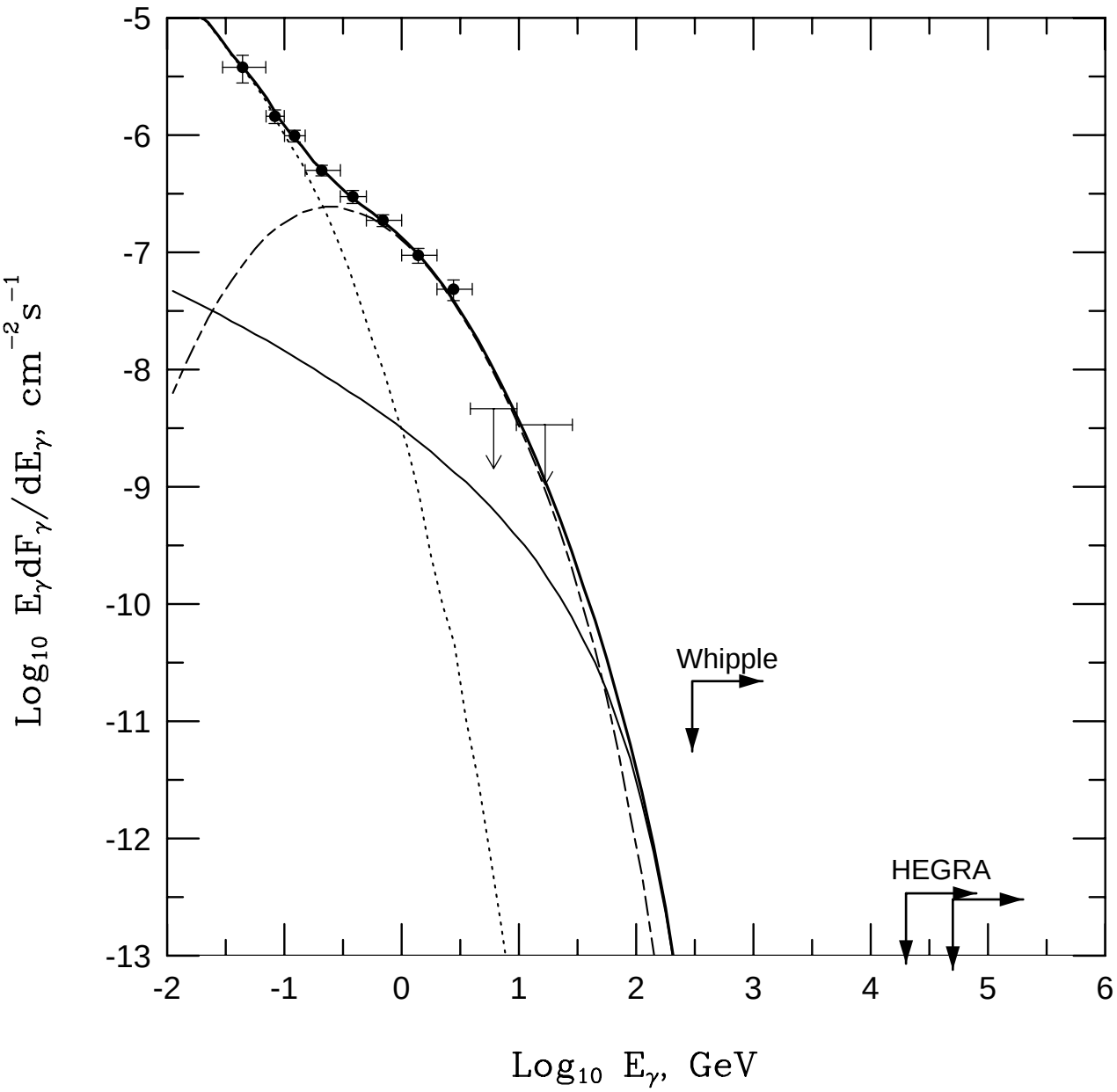

Fig. 8.— Best fit (Fit 4) of γ Cygni.

Gaisser, Protheroe & Stanev, Fig. 8, gCygni Fit 4